2023-12-28

An *In-Situ* Raman Spectroscopic Study on the Interfacial Process of Carbonate-Based Electrolyte on Nanostructured Silver Electrode

Yu Gu
State Key Laboratory of Physical Chemistry of Solid Surfaces, Innovation Laboratory for Sciences and Technologies of Energy Materials of Fujian Province (IKKEM), College of Chemistry and Chemical Engineering, Xiamen University, Xiamen 361005, Fujian, China, ygu@xmu.edu.cn

Yuan-Fei Hu

Wei-Wei Wang

En-Ming You

Shuai Tang

Jian-Jia Su

Jun Yi

See next page for additional authors

An *In-Situ* Raman Spectroscopic Study on the Interfacial Process of Carbonate-Based Electrolyte on Nanostructured Silver Electrode

Authors

Yu Gu, Yuan-Fei Hu, Wei-Wei Wang, En-Ming You, Shuai Tang, Jian-Jia Su, Jun Yi, Jia-Wei Yan, Zhong-Qun Tian, and Bing-Wei Mao

Corresponding Author(s)

Yu Gu(ygu@xmu.edu.cn);
Bing-Wei Mao (bwmao@xmu.edu.cn)

ORIGINAL ARTICLE

An *In-Situ* Raman Spectroscopic Study on the Interfacial Process of Carbonate-Based Electrolyte on Nanostructured Silver Electrode

Yu Gu [a,#,*], Yuan-Fei Hu [a,#], Wei-Wei Wang [a], En-Ming You [a], Shuai Tang [a,b], Jian-Jia Su [a], Jun Yi [a], Jia-Wei Yan [a], Zhong-Qun Tian [a], Bing-Wei Mao [a,*]

[a] State Key Laboratory of Physical Chemistry of Solid Surfaces, Innovation Laboratory for Sciences and Technologies of Energy Materials of Fujian Province (IKKEM), College of Chemistry and Chemical Engineering, Xiamen University, Xiamen 361005, Fujian, China
[b] College of Chemistry, Zhengzhou University, Zhengzhou 450001, Fujian, China

Abstract

The solid-electrolyte interphase (SEI) plays a key role in anodes for rechargeable lithium-based battery technologies. However, a thorough understanding in the mechanisms of SEI formation and evolution remains a major challenge, hindering the rapid development and wide applications of Li-based batteries. Here, we devise a borrowing surface-enhanced Raman scattering (SERS) activity strategy by utilizing a size optimized Ag nanosubstrate to *in-situ* monitor the formation and evolution of SEI, as well as its structure and chemistry in an ethylene carbonate-based electrolyte. To ensure a reliable *in-situ* SERS investigation, we designed a strict air-tight Raman cell with a three-electrode configuration. Based on the potential-dependent spectroscopic information, we revealed that the SEI formed in an EC-based electrolyte presents a double-layer structure, comprising a thin inorganic inner layer and an organic-rich outer layer. We also identified that LEMC, rather than LEDC, is the major component of EC reduction, and the critical role of metallic Li in the formation of stable SEI is preliminary explored. Nevertheless, identifying the SEI compositions is only feasible before Li deposition on the Ag surface. After the formation of Li-Ag alloys, the subsequent evolution of SEI could not be detected due to the change in the dielectric constant of Ag after the lithiation. Our work provides a real-time spectroscopic method for investigating interfacial processes of anodes, which is beneficial to the understanding of SEI formation and evolution and thus provides guidance for the development of rationally designed SEI in Li-based batteries.

Keywords: Solid-electrolyte interphase; *In-situ* SERS; Anodes; Lithium-based batteries

1. Introduction

Motivated by the ever-increasing demand for high performances, understanding the processes at the electrode/electrolyte interfaces has become a paramount factor for the success of rechargeable lithium-based battery technologies, including Li-ion and Li-metal batteries [1−3]. Focusing on the anode side, the solid-electrolyte interphase (SEI), functioning as an electronic insulator but a Li-ionic conductor, is inevitably formed on the anode surface as a result of (electro-)chemical electrolyte reduction during charge-discharge cycling [4,5]. Such an interphase is a nanometric-thin layer composed of various organic/inorganic species, which is responsible for not only impeding the continuous parasitic reactions of electrolyte decomposition, but also determining the mass flow

and electrochemical kinetics of the anode closely related to the cycle performance of a Li-based battery [6−8]. Therefore, a thorough understanding in the formation and evolution of SEIs is of prime importance towards the achievement of high-performance Li-based batteries.

Since the independent pioneering works by Peled et al. and Aurbach et al., several SEI structural models, including the prevailing mosaic mode and multilayer mode, have been proposed based on the results obtained from various characterization techniques combined with theoretical simulations [9−14]. Regardless of the discrepancies in terms of detailed structure, the SEI is generally regarded to be a mosaic assembly of the different inorganic and organic components, arranged in a configuration with a compact inorganic-rich inner layer and a loose organic-rich outer layer [9,12]. Moreover, the SEI may experience further dynamic evolution during the battery operation, which is complicated by electrolyte composition and formation conditions [15−17]. Although these findings have contributed to the understanding of SEI, many critical questions associated with the formation and growth mechanisms of SEI as well as the impacts of its structures and properties on the battery performance remain poorly answered, which hinders rational design and optimization of the anode/electrolyte interfaces for Li-based batteries. Therefore, *in-situ* and real-time structure-specific methods that enable nondestructive monitoring the SEI formation and evolution, as well as the identification of the possible functions of SEI components, are indispensable to comprehensively understand the complicated structure and chemistry of such key interphase and its coupled interface in battery systems.

Surface-enhanced Raman spectroscopy (SERS) is an extremely surface-sensitive vibrational spectroscopy, in which the Raman signals of analytes under investigation near nanostructures of some metals such as Au, Ag and Cu are amplified by several orders of magnitude via the excitation of the localized surface plasmons (LSPs) from those nanostructures [18−20]. It is recognized as a powerful fingerprint technique and have been applied for *in-situ* studies of a variety of electrochemical interfaces [21−23]. As the two important variants of SERS, tip-enhanced Raman spectroscopy (TERS) and shell-isolated nanoparticle-enhanced Raman spectroscopy (SHINERS) offer a feasible solution of achieving giant enhanced Raman signals from unperturbed surfaces of general materials, which provide a great opportunity to follow electrochemical reactions on a wide range of electrode surfaces [24−26]. Starting from 2000,

these techniques have been applied to investigate the interfacial processes of batteries at the molecular level [27−35]. However, most of the studies have focused on the cathode sides of Li-based batteries, involving oxygen electrode electrochemistry and surface changes of cathode materials. Only a few researches have been dedicated to identifying the composition and structure of SEIs on anodes, mostly silicon-based anodes. The general difficulty may lie in the fact that the signals of nanometric thick SEI is extremely weak and influenced by many factors, so that the effective borrowing SERS activity strategy from highly SERS-active substrates needs to be implemented in operation [36,37]. Meanwhile, such measurements must be performed in an inert atmosphere, and the design of moisture- and oxygen-free electrochemical Raman cell is also particularly important to avoid bringing additional complexity in operation. On the other hand, SERS enhancement effects are inherently dependent on the morphologies and structures of SERS-active substrates [18,19,38]. In the previous SERS studies on Li-based battery systems, the roughened metal surfaces with random nanostructures and a broad size distribution of hotspots (i.e., nanoscale regions with extraordinarily large local electromagnetic field) were typically employed as the SERS substrates [27,30]. Although it has been demonstrated to be capable of probing the interfacial processes, the availability of such substrates with less efficiency and stability is still a major challenge toward the widespread and practical use of SERS in battery field. Thus, a uniform substrate with specific nanostructures in close proximity to each other, such as nanoparticle arrays, is highly required to achieve a homogeneous and reproducible Raman signal enhancement, which enables the facile utilization of SERS in following interface chemistry within Li-based batteries.

In this work, we employed *in-situ* SERS to characterize the formation and evolution of SEI in an EC-based carbonate electrolyte. The Ag electrode modified with the size optimized Ag nanoparticles, possessing the excellent LSP efficiency and wide LSP response in the visible region amongst the coinage metals [39,40], was used as the high-efficient SERS-active substrate for *in-situ* probing the SEI formation processes, and elucidating the structure and chemistry of SEI. Our results show advantages of investigations by SERS for more accurate and real-time characterization of the structure and chemistry of SEIs, which facilitates an in-depth and a comprehensive understanding of SEI and its impacts on performance of anodes for Li-based batteries.

2. Experimental section

2.1. Preparation of Ag nanoparticles

The Ag nanoparticles were synthesized via an Au-seed growth method following previous reports [40,41]. First, Au-seed nanoparticles with a diameter of ca. 10 nm were prepared using the sodium citrate reduction method. 100 mL of $HAuCl_4$ aqueous solution (0.01 wt%) was heated to boiling under string. 3 mL of sodium citrate aqueous solution (1 wt%) was quickly added to the above boiling solution and refluxed for 30 min. The obtained sanguine Au sol was allowed to cool to ambient conditions for the next step. Then, $AgNO_3$ was subsequently reduced on Au-seeds using sodium citrate with ascorbic acid the reducing agent and stabilizing agent. 0.5 mL of the Au sol was dispersed into 20 mL of deionized water serving as the seed solution. 0.5 mL of sodium citrate aqueous solution (1 wt%) was added to the seed solution, and followed by adding 3 mL of ascorbic acid (10 mmol·L^{-1}). 2.8 mL of $AgNO_3$ solution (10 mmol·L^{-1}) was then added dropwise at a rate of one drop every 5−10 s, which was followed by the addition of another 1.5 mL of sodium citrate aqueous solution (1 wt%). After 10 min of light-avoidance-stirring, the Ag sol with diameter of ca. 100 nm was obtained. The as-prepared Ag nanoparticles were centrifuged thrice and washed with deionized water for later use. The overall morphology of Ag nanoparticles was characterized by scanning electron microscope (SEMHITACHI, S-4800) at an accelerating voltage of 15 kV.

2.2. Assembly of Ag nanoparticles on Ag electrode and the cleaning process

An Ag disc ($\Phi = 0.5$ mm) was used as the electrode substrate. Before assembly, the Ag electrode was successively polished with alumina powder of 1.0, 0.3 and 0.05 μm on the microcloths to ensure a fresh and smooth electrode surface, which was followed by rinsing thoroughly with ultrapure water and cleaning ultrasonically before modifying the surface. For the assembly of Ag nanoparticles on the clean surface of the Ag electrode, the above concentrated Ag sol was diluted with 0.5 mL of deionized water to make up a stock solution. Two microliters of the stock solution were then drop-cast onto the surface of Ag electrode and subsequently dried under vacuum. For the cleaning process, the Ag electrode modified with Ag nanoparticles was placed in an electrochemical cell (Pt wire as the counter electrode) filled with 0.1 mol·L^{-1} Ar-saturated $NaClO_4$ aqueous solution, and polarized at −1.2 V (vs. SCE) for about 1−2 min, during which the generation of tiny hydrogen bubbles could be observed [42]. The hydrogen evolution reaction (HER) proceeded vigorously, so that the impurities adsorbed on the Ag nanoparticles or electrode surface were desorbed and diffused into the solution. This procedure was repeated 3−5 times, accompanied by changing the fresh $NaClO_4$ solution. Finally, the modified Ag electrode was rapidly transferred to drying oven and dried under vacuum overnight for later use.

2.3. In-situ SERS measurements

In-situ SERS measurements were conducted on a Raman-11 system (Nanophoton) equipped with a 50 × (NA 0.45) objective and a 600 grooves/mm grating. A commercial carbonate electrolyte of 1 mol·L^{-1} $LiPF_6$/EC-DMC (vol:vol = 2:1) commonly used in Li-based batteries was chosen as the electrolyte solution. A homemade sealed three-electrode Raman cell coupled with an electrochemical workstation to control the potential, in which Ag electrode modified with Ag nanoparticles served as the working electrode and Li strips served as both the reference and counter electrodes, was assembled in an Ar-filled glovebox (<0.1 ppm of H_2O and O_2). The working electrode surface faced upwards and towards a quartz glass window of the cell with 0.5 mm thickness. A thin liquid layer (<100 μm) was trapped between the electrode surface and quartz window to ensure that the Raman signals were from the metal-SEI interface, instead of the bulk electrolyte. The 532 nm laser was chosen with a local power at electrode of approximately 0.02 mW·μm^{-2} and the acquisition time was 60 s for each spectrum. Raman frequencies were calibrated using a Si wafer.

2.4. Theoretical simulation

The simulated electromagnetic field is obtained by commercial simulation software (COMSOL Multiphysics) based on the finite element method. A spherical simulation domain, whose diameter is 2.502 μm, is created, and perfectly matched layers (PMLs) are employed to simulate an open boundary. The bottom half of the simulation domain is set as Ag. The medium over the Ag substrate is set to be the electrolyte. Two spherical Ag nanoparticles, whose diameters are 100 nm, are buried in the Ag substrate. The size of the nanogap is 2 nm for the adjacent Ag nanoparticles. The minimal mesh size is 0.5 nm in close proximity to the nanoparticles and gradually becomes coarser towards the borders of the simulation domain. The refractive indexes of the electrolyte are 1.4 [43]. The permittivity values for Ag and Li are taken from literatures [44,45].

3. Results and discussion

Fig. 1a shows the SEM image of the Ag nanoparticles. The nanoparticles prepared in this work are generally of quasi-spherical shape. The statistical analysis demonstrates that the average diameter of the Ag nanoparticles is ca. 110 nm (Fig. 1b). The Ag nanoparticles were assembled on the Ag electrode for SERS investigations. To overcome the undesirable electrochemical responses and Raman signals originating from the impurities, such as sodium citrate, the modified Ag electrode was cleaned by HER procedure in a deoxygenated $NaClO_4$ solution. The corresponding Raman spectra recorded on the modified Ag electrode before and after HER are shown in Fig. 1c. It is seen that the bands at ca. 500 cm^{-1} and 1100−1700 cm^{-1} associated with impurities (e.g., residual sodium citrate) are absent in Raman spectra after cleaning processes, demonstrating the efficiency of such HER cleaning protocol. Fig. 1d shows the result for the distribution of electric field strength surrounding the modified Ag electrode under 532 nm excitation modelled using a finite-element method (FEM). The hotspots are located around the particle-electrode and particle-particle junctions, and the average SERS enhancement

factor of this configuration reaches up to 10^{10}, which is theoretically strong enough for ultrasensitive detection of SEI formation.

To ensure a reliable *in-situ* SERS investigation, we designed an air- and water-tight Raman cell with three-electrode configuration so that the potential can be precisely controlled during the measurement (Fig. 2a). The tightness of the customized cell was first checked by using p-aminothiophenol (PATP) as a probe molecule, which could be rapidly oxidized to p,p'-dimercaptoazobenzene (DMAB) on Ag nanoparticles in an air atmosphere in the presence of LSP [46]. The modified Ag electrode was pre-adsorbed with PATP and sealed into the Raman cell in an Ar-filled glovebox where both O_2 and H_2O were below 0.1 ppm. The sealed cell was then transferred to Raman equipment for measurement in an air atmosphere. The time-dependent Raman spectra of modified Ag electrode with PATP are shown in Fig. 2b. It is seen that the initial Raman spectrum displays strong and characteristic bands associated with PATP. After 6 h, the recorded Raman spectrum shows no significant change compared to the initial one. However, the bands at 1140, 1388 and 1434 cm^{-1} associated with DMAB [46] can be
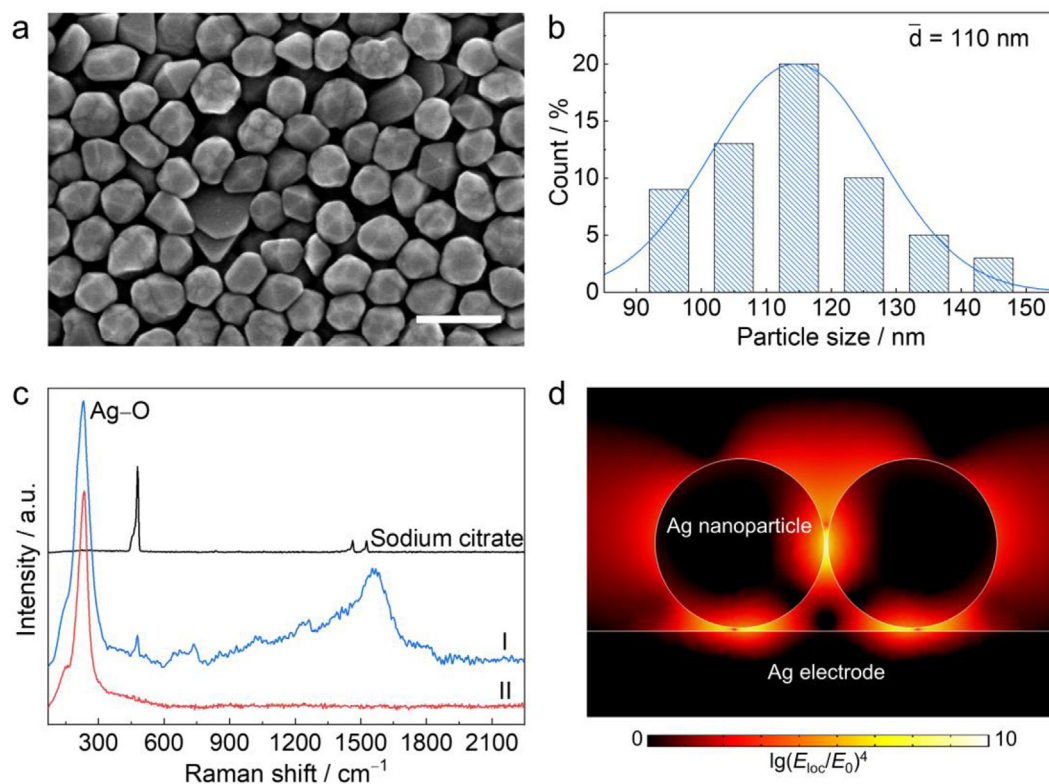

Fig. 1. (a) SEM image of Ag nanoparticles. Scale bar: 200 nm. (b) The size distribution of Ag nanoparticles. (c) Raman spectra of sodium citrate and the modified Ag electrode before (I) and after (II) HER. (d) Finite-element simulations of the electromagnetic field distribution of the modified Ag electrode. E_{1oc} and E_0 represent the localized field and the incident field, respectively.
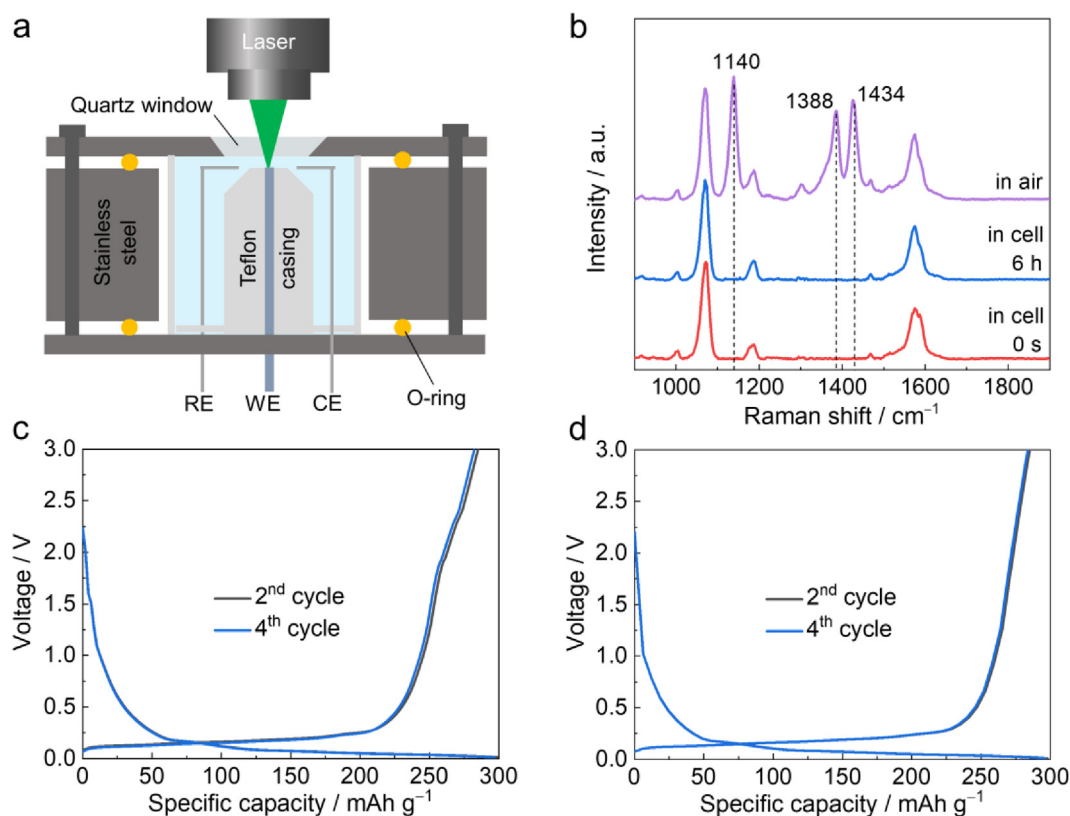
Fig. 2. (a) Schematic of an air-tight in-situ Raman cell with three-electrode configuration. (b) Time-dependent Raman spectra of PATP absorbed on the modified Ag electrode. (c, d) Charge-discharge curves of graphite electrode measured in the sealed Raman cell (c) and glovebox (d).

clearly observed after the Raman cell was disassembled and exposed to air. These results indicate that the customized Raman cell is strict airtight. The tightness and applicability of the cell were also examined by galvanostatic charge-discharge cycling test of graphite. As shown in Fig. 2c and d, the charge-discharge curves of the graphite electrode within the Raman cell tested in the glovebox and Raman cell are in close agreement, again demonstrating the favorable tightness of the Raman cell, and thus the Raman cell is suitable for *in-situ* monitoring the SEI formation and evolution, and elucidating the structure and chemistry of SEI.

The electrochemical behaviors of 1 mol·L^{-1} LiPF$_6$/EC-DMC were investigated by cyclic voltammetry (CV) as shown in Fig. 3. Since the lower limit of the cathodic scan was set to 0.0 V vs. Li/Li$^+$, there was no Li overpotential deposition in these CVs. The reduction peak at ca. 2.0 V is correlated to the reduction of trace H$_2$O, which is extremely difficult to be avoided in the electrolyte [47]. As the potential was scanned negatively, the main electrolyte reduction was initiated at ca. 1.5 V, which is proposed to be assigned mainly to the reduction of EC solvent [48]. Following the Li underpotential deposition (UPD) at around 0.65 V, Li-Ag alloying

process might take place at ca. 0.2 V [49]. The formation of Li-Ag alloys could hamper the detection of SEI evolution at this stage, which is discerned by the significantly lessened Raman signals in the follow-up *in-situ* Raman study. A more detailed discussion will be given later. The electrolyte reduction became absent in the follow-up cycles, indicating that the passivation of electrode is achieved after the first cycles.

To monitor the formation and evolution of SEI, the *in-situ* SERS measurement was performed on
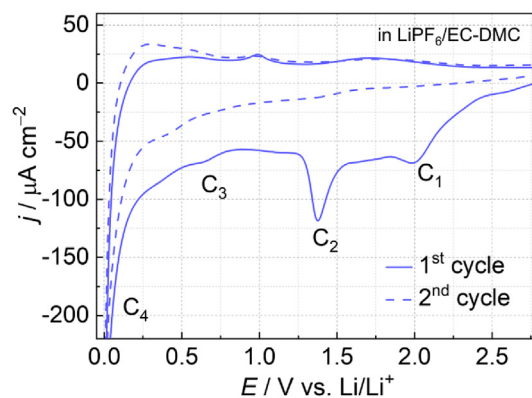

Fig. 3. CV curves of the Ag electrode modified with Ag nanoparticles in 1 mol·L^{-1} LiPF$_6$/EC-DMC (2/1, V/V). Scan rate: 20 mV s^{-1}.

the modified Ag electrode at different potentials scanning from 2.8 to 0.0 V (Figs. 4 and 5). The assignments of bands associated with SEI species are summarized in Table S1. At the potentials negative to 2.0 V, the features of surface Raman spectra resemble those of bulk electrolyte while a few significant changes in the regions of 700−750 and 850−950 cm^{-1} (Fig. 4), which indicates an
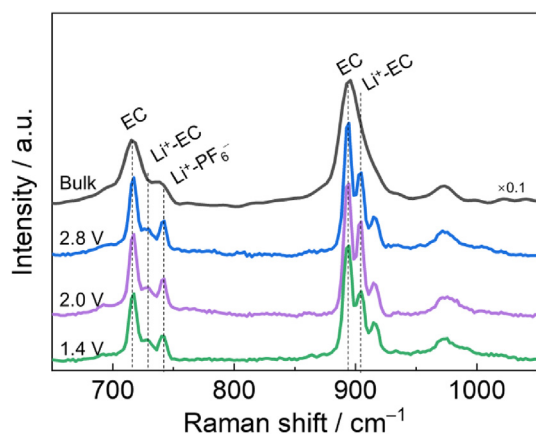

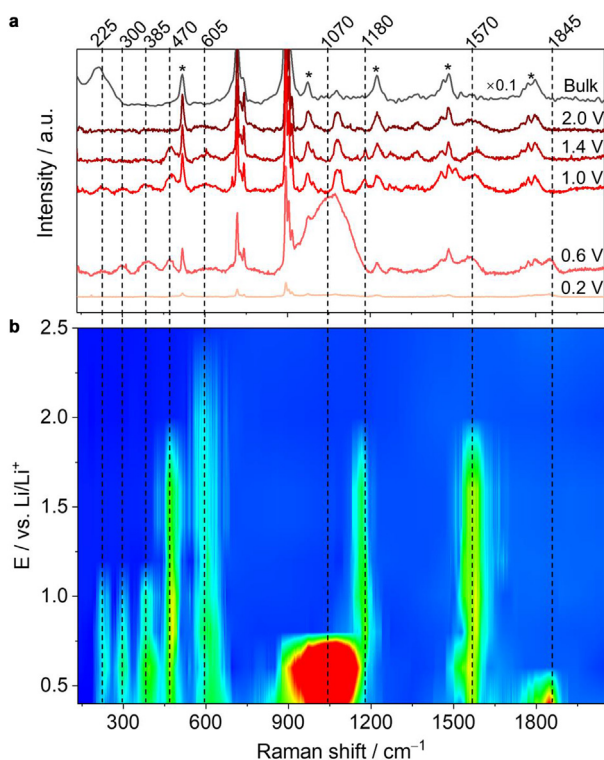*Fig. 4. Raman spectra of bulk electrolyte of LiPF$_6$/EC-DMC and SERS spectra of LiPF$_6$/EC-DMC on the modified Ag electrode at different potentials.*

Fig. 5. (a) In-situ SERS spectra of SEI formation on the Ag electrode modified with Ag nanoparticles in 1 mol·L^{-1} LiPF$_6$/EC-DMC. (b) The 2D color map representing the Raman band as a function of the applied potential allows an appreciation of the dynamics of SEI compositions.

interaction between electrolyte and Ag surface. Specifically, the apparent monolithic bands originating from ring breathing and C−C stretching modes of EC in these regions [50] split into several bands, among of which the vibrational bands of Li$^+$-coordinated EC (728 and 903 cm^{-1}) and Li$^+$-coordinated PF$_6^-$ (742 cm^{-1}) became discriminable and slightly more intense relative to those in bulk electrolyte upon decrease of the potential to 2.0 V. This can be explained by the adsorption of Li$^+$-coordinated EC/PF$_6^-$ in the inner Helmholtz layer of the electric double layer at the charged Ag surface [28]. Meanwhile, a broad band at ca. 605 cm^{-1} related to the LiF species is observed due to the PF$_6^-$ reduction at this potential. With the negative shifting of potential to below 2.0 V, however, the SERS spectra changed obviously as a function of potential, correlating with the initiation of solvent reduction and thus the formation of SEI.

As presented in Fig. 5, when the potential was held at 1.4 V, several new bands at 470, 1180 and ca. 1570 cm^{-1} appear synchronously, which are attributed to the C−O stretching mode and C−H bending mode of ROCO$_2$Li that could be originated from the reduction and polymerization of EC solvent. These peaks still gradually grew upon negative potential excursion, suggesting the continuous accumulation of this species in SEI. Simultaneously, the new bands at ca. 225, ca. 300 and ca. 385 cm^{-1} are observed initially at 1.0 V. These lower frequency bands are characteristic vibration modes of the inorganic LiF and LiOH species. The SERS spectrum changed dramatically when the potential moved negatively to 0.6 V where electrolyte reduction with concurrent Li UPD took place. A strong and overlapping broad band emerged at ca. 1070 cm^{-1} and it remained present throughout the remaining potentials before 0.2 V. This indicates that new amorphous species associated with lithium alkyl carbonates and LiF formed on SEI as soon as the Li UPD occurred at a significant rate. Interestingly, however, the evolution of the SERS spectra shows a dramatic decrease in intensity at 0.2 V and more negative potentials, where Li-Ag alloying process occurred. The formation of Li-Ag alloys presumably weakened the SERS enhancement effects of the modified Ag electrode, which results in weaker scattering of the Raman signals associated with SEI. To better assess the plasmonic properties of Li-Ag alloys and their impacts on the electromagnetic field distribution, FEM simulations are carried out for the modified Ag electrode with different Li-Ag alloying degrees. As shown in Fig. 6, upon the increase in the degree of the Li-Ag alloying, the average SERS enhancement factor of
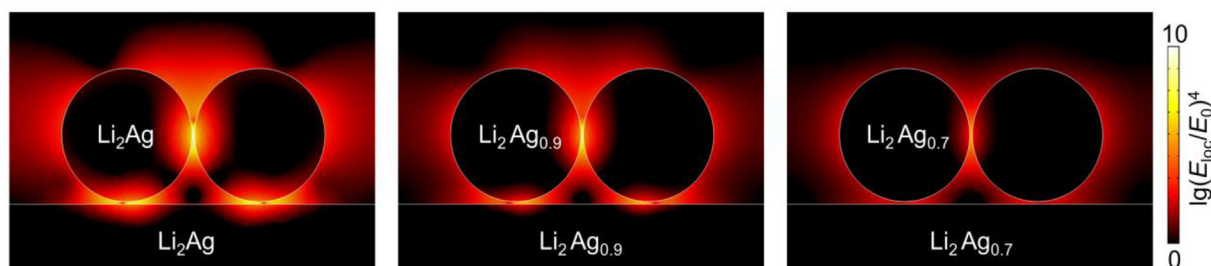
Fig. 6. Finite-element simulations of the electromagnetic field distribution of the modified Ag electrode during Li-Ag alloying processes. E_{1oc} and E_0 represent the localized field and the incident field, respectively.

the modified Ag electrode keeps weakening and reaches its minimum when the $Li_2Ag_{0.7}$ alloy is developed, which confirms that the formation of Li-Ag alloys is unfavorable for the SERS enhancement. This could be ascribed to the significant change in dielectric constant of Li-Ag alloy compared to Ag itself under the laser excitation at the same wavelength (Fig. S1), which remains to be investigated further.

The above potential-dependent SERS study provides important molecular-level chemical information for analysis and understanding of SEI formation and evolution in carbonate electrolyte. Several pieces of insights can be drawn from these as follows. First, the observations on the evolution of various Raman bands as a function of potential described above firmly indicate a structured SEI that comprises a thin inorganic inner layer composed of LiF and LiOH and an organic-rich outer layer. Such SEI falls within the framework of mosaic-type double-layer mode of SEI [9,10]. Second, the lithium alkyl carbonates are considered as the major organic SEI components originating from EC reduction and polymerization, but controversies still exist about the specific categories of carbonates. Since proposed by Aurbach and coworkers in 1996, it has been recognized that lithium ethylene dicarbonate (LEDC) is a primary product from EC reduction [51]. While Wang et al. have observed different phenomena in 2019 and challenged the previous understanding by asserting that lithium ethylene monocarbonate (LEMC) was believed to be the product from EC rather than LEDC [52]. In the present work, a broad band at approximately 1070 cm^{-1} was detected when EC reduction with concurrent Li UPD took place. Deconvolution analysis shows that the band agrees with LEMC by comparison of reference Raman spectra of LEDC and LEMC [33] (Fig. S2), suggesting that LEMC is more likely to be the major component in SEI. This result is consistent with the mechanisms and conclusions proposed by Wang et al. that the formation of LEMC may be attributed to the interconversions of unstable organic components in SEI. Third, the

formation of more stable LEMC could be highly related to the presence of metallic Li after Li UPD, although only atomic-layered Li occurs on Ag surface. It seems that unstable species would be further converted via additional (electro-)chemical reactions under supply of active metallic Li and the broadened shapes of the vibrational bands indicate that the SEI on Li surface may be amorphous, which is still fully understood and needs further work. Finally, noteworthy is that the formation of Li-Ag alloy can weaken the SERS enhancement effects of Ag electrode, and thus reducing the detection sensitivity to the SEI formed on Li surface. Regardless of that, the successful tracking of the SEI composition before Li deposition is still desirable for revealing the formation mechanism of SEI and thus providing guidance in the design of SEIs especially in Li-ion batteries.

4. Conclusions

In summary, we employed the borrowing SERS activity strategy from highly SERS-active Ag substrate to *in-situ* probe the SEI formation and evolution, and the corresponding structure and chemistry of SEI in an EC-based carbonate electrolyte. It is found that the identification of the SEI compositions can be easily done only before the formation of Li-Ag alloy on SERS-active Ag substrate. However, based on the chemical information obtained in a limited potential range, we unraveled that the SEI formed in EC-based electrolyte presents a double-layer structure that consists of a thin inorganic inner layer and an organic-rich outer layer. We also excluded that LEMC is the major component of EC reduction rather than LEDC, and the critical role of metallic Li in the formation of stable SEI was preliminary explored. Our work establishes the correlation between the potential and the structure and chemistry of SEI formed in the carbonate electrolyte, showing a relatively complete picture of SEI formation and evolution. These results will provide guidance for development of rationally designed SEI in

Li-based batteries. Further investigations should be carried out by optimizing around the configuration of SERS-active substrate to increase the detection sensitivity to SEI for more desirable characterization of the complex interfacial processes in Li-based batteries. The implementation of SHINER complement SERS would be a promising direction for revealing the formation mechanism of SEI on the Li surface.

Acknowledgements

References

[1] Atkins D, Ayerbe E, Benayad A, Capone F G, Capria E, Castelli I E, Cekic-Laskovic I, Ciria R, Dudy L, Edström K, Johnson M R, Li H, Lastra J MG, De Souza M L, Meunier V, Morcrette M, Reichert H, Simon P, Rueff J P, Sottmann J, Wenzel W, Grimaud A. Understanding battery interfaces by combined characterization and simulation approaches: challenges and perspectives[J]. Adv. Energy Mater., 2021, 12(17): 2102687.

[2] Yu X, Manthiram A. Electrode-electrolyte interfaces in lithium-based batteries[J]. Energy Environ. Sci., 2018, 11(3): 527−543.

[3] Yan C, Xu R, Xiao Y, Ding J F, Xu L, Li B Q, Huang J Q. Toward critical electrode/electrolyte interfaces in rechargeable batteries[J]. Adv. Funct. Mater., 2020, 30(23): 1909887.

[4] Peled E. The electrochemical behavior of alkali and alkaline earth metals in nonaqueous battery systems—the solid electrolyte interphase model[J]. J. Electrochem. Soc., 1979, 126(12): 2047−2051.

[5] Peled E, Menkin S. Review—SEI: past, present and future [J]. J. Electrochem. Soc., 2017, 164(7): A1703−A1719.

[6] Xu R, Yan C, Huang J Q. Competitive solid-electrolyte interphase formation on working lithium anodes[J]. Trends Chem., 2021, 3(1): 5−14.

[7] Gu Y, Wang W W, Li Y J, Wu Q H, Tang S, Yan J W, Zheng M S, Wu D Y, Fan C H, Hu W Q, Chen Z B, Fang Y, Zhang Q H, Dong Q F, Mao B W. Designable ultra-smooth ultra-thin solid-electrolyte interphases of three alkali metal anodes[J]. Nat. Commun., 2018, 9(1): 1339.

[8] Cheng X B, Zhang R, Zhao C Z, Zhang Q. Toward safe lithium metal anode in rechargeable batteries: a review[J]. Chem. Rev., 2017, 117(15): 10403−10473.

[9] Aurbach D, Zaban A. Impedance spectroscopy of lithium electrodes. 1. General behavior in propylene carbonate solutions and the correlation to surface-chemistry and cycling efficiency[J]. J. Electroanal. Chem., 1993, 348(1−2): 155−179.

[10] Peled E, Golodnitsky D, Ardel G. Advanced model for solid electrolyte interphase electrodes in liquid and polymer electrolytes[J]. J. Electrochem. Soc., 1997, 144(8): L208−L210.

[11] Gu Y, Wang W W, Yan J W, Wu D Y, Dong Q F, Mao B W. Surface electrochemistry approaches for understanding and creating smooth solid-electrolyte interphase and lithiophilic interfaces for lithium metal anodes[J]. Curr. Opin. Electrochem., 2021, 26: 100671.

[12] Wu H, Jia H, Wang C, Zhang J G, Xu W. Recent progress in understanding solid electrolyte interphase on lithium metal anodes[J]. Adv. Energy Mater., 2020, 11(5): 2003092.

[13] Wang A P, Kadam S, Li H, Shi S Q, Qi Y. Review on modeling of the anode solid electrolyte interphase (SEI) for lithium-ion batteries[J]. npj Comput. Mater., 2018, 4(1): 15.

[14] Wang W W, Gu Y, Yan H, Li S, He J W, Xu H Y, Wu Q H, Yan J W, Mao B W. Evaluating solid-electrolyte interphases for lithium and lithium-free anodes from nanoindentation features[J]. Chem, 2020, 6(10): 2728−2745.

[15] Wang W W, Gu Y, Wang J H, Chen Z B, Yin X T, Wu Q H, Yan J W, Mao B W. Probing mechanical properties of solid-electrolyte interphases on Li nuclei by *in situ* AFM[J]. J. Electrochem. Soc., 2022, 169(2): 020563.

[16] Wang W W, Gu Y, Yan H, Li K X, Chen Z B, Wu Q H, Kranz C, Yan J W, Mao B W. Formation sequence of solid electrolyte interphases and impacts on lithium deposition and dissolution on copper: an *in situ* atomic force microscopic study[J]. Faraday Discuss, 2022, 233: 190−205.

[17] Lin D C, Liu Y Y, Li Y B, Li Y Z, Pei A, Xie J, Huang W, Cui Y. Fast galvanic lithium corrosion involving a Kirkendall-type mechanism[J]. Nat. Chem., 2019, 11(4): 382−389.

[18] Ding S Y, Yi J, Li J F, Ren B, Wu D Y, Panneerselvam R, Tian Z Q. Nanostructure-based plasmon-enhanced Raman spectroscopy for surface analysis of materials[J]. Nat. Rev. Mater., 2016, 1(6): 16021.

[19] Panneerselvam R, Liu G K, Wang Y H, Liu J Y, Ding S Y, Li J F, Wu D Y, Tian Z Q. Surface-enhanced Raman spectroscopy: bottlenecks and future directions[J]. Chem. Commun., 2018, 54(1): 10−25.

[20] Wu D Y, Li J F, Ren B, Tian Z Q. Electrochemical surface-enhanced Raman spectroscopy of nanostructures[J]. Chem. Soc. Rev., 2008, 37(5): 1025−1041.

[21] Weiling M, Pfeiffer F, Baghernejad M. Vibrational spectroscopy insight into the electrode|electrolyte interface/interphase in lithium batteries[J]. Adv. Energy Mater., 2022, 12(46): 2202504.

[22] Shen Y F, Chen Y L, Wang S X, Zhu Y, Wang W C, Wu M X, Chen Z D. Electrochemical SERS study of Benzotriazole and 3-mercapto-1-propanesulfonate in acidic solution on copper electrode[J]. J. Electrochem., 2022, 28(6): 2104451.

[23] Peng H Y, Wang J Z, Liu J, Yu H H, Lin J D, Wu D Y, Tian Z Q. Investigation on electrochemical processes of p-aminothiophenol on gold electrode of nanostructures[J]. J. Electrochem., 2022, 28(4): 2106281.

[24] Li J F, Huang Y F, Ding Y, Yang Z L, Li S B, Zhou X S, Fan F R, Zhang W, Zhou Z Y, Wu D Y, Ren B, Wang Z L, Tian Z Q. Shell-isolated nanoparticle-enhanced Raman spectroscopy[J]. Nature, 2010, 464(7287): 392−395.

[25] Su M, Dong J C, Li J F. *In-situ* Raman spectroscopic study of electrochemical reactions at single crystal surfaces[J]. J. Electrochem., 2020, 26(1): 54−60.

[26] Wang X, Huang S C, Huang T X, Su H S, Zhong J H, Zeng Z C, Li M H, Ren B. Tip-enhanced Raman spectroscopy for surfaces and interfaces[J]. Chem. Soc. Rev., 2017, 46(13): 4020−4041.

[27] Li H, Mo Y J, Pei N, Xu X X, Huang X J, Chen L Q. Surface-enhanced Raman scattering study on passivating films of Ag electrodes in lithium batteries[J]. J. Phys. Chem. B, 2000, 104(35): 8477−8480.

[28] Gogoi N, Melin T, Berg E J. Elucidating the step-wise solid electrolyte interphase formation in lithium-ion batteries

with operando Raman spectroscopy[J]. Adv. Mater. Interf., 2022, 9(22): 2200945.

[29] Tang S, Gu Y, Yi J, Zeng Z, Ding S Y, Yan J W, Wu D Y, Ren B, Tian Z Q, Mao B W. An electrochemical surface-enhanced Raman spectroscopic study on nanorod-structured lithium prepared by electrodeposition[J]. J. Raman Spectrosc., 2016, 47(9): 1017−1023.

[30] Johnson L, Li C, Liu Z, Chen Y, Freunberger S A, Ashok P C, Praveen B B, Dholakia K, Tarascon J M, Bruce P G. The role of LiO_2 solubility in O_2 reduction in aprotic solvents and its consequences for $Li-O_2$ batteries[J]. Nat. Chem., 2014, 6(12): 1091−1099.

[31] Wang J W, Zhang Y L, Guo L M, Wang E K, Peng Z Q. Identifying reactive sites and transport limitations of oxygen reactions in aprotic lithium-O_2 batteries at the stage of sudden death[J]. Angew. Chem. Int. Ed., 2016, 55(17): 5201−5205.

[32] Hy S, Felix F, Rick J, Su W N, Hwang B J. Direct *in situ* observation of Li_2O evolution on Li-rich high-capacity cathode material, $Li[Ni_x li_{(1−2x)/3} mn_{(2−x)/3}]O_2$ ($0 \leq x \leq 0.5$)[J]. J. Am. Chem. Soc., 2014, 136(3): 999−1007.

[33] Gajan A, Lecourt C, Torres Bautista B E, Fillaud L, Demeaux J, Lucas I T. Solid Electrolyte interphase instability in operating lithium-ion batteries unraveled by enhanced-Raman spectroscopy[J]. ACS Energy Lett., 2021, 6(5): 1757−1763.

[34] Nanda J, Yang G, Hou T, Voylov D N, Li X, Ruther R E, Naguib M, Persson K, Veith G M, Sokolov A P. Unraveling the nanoscale heterogeneity of solid electrolyte interphase using tip-enhanced Raman spectroscopy[J]. Joule, 2019, 3(8): 2001−2019.

[35] Zhang W L, Lu Y, Wan L, Zhou P, Xia Y C, Yan S S, Chen X X, Zhou H Y, Dong H, Liu K. Engineering a passivating electric double layer for high performance lithium metal batteries[J]. Nat. Commun., 2022, 13(1): 2029.

[36] Tian Z Q, Ren B, Li J F, Yang Z L. Expanding generality of surface-enhanced Raman spectroscopy with borrowing SERS activity strategy[J]. Chem. Commun. 2007;(34): 3514−3534.

[37] Li J F, Zhang Y J, Ding S Y, Panneerselvam R, Tian Z Q. Core-shell nanoparticle-enhanced Raman spectroscopy[J]. Chem. Rev., 2017, 117(7): 5002−5069.

[38] Sharma B, Frontiera R R, Henry A I, Ringe E, Van Duyne R P. SERS: materials, applications, and the future[J]. Mater. Today, 2012, 15(1−2): 16−25.

[39] Hutter E, Fendler J H. Exploitation of localized surface plasmon resonance[J]. Adv. Mater., 2004, 16(19): 1685−1706.

[40] Uzayisenga V, Lin X D, Li L M, Anema J R, Yang Z L, Huang Y F, Lin H X, Li S B, Li J F, Tian Z Q. Synthesis, characterization, and 3D-FDTD simulation of $Ag@SiO_2$ nanoparticles for shell-isolated nanoparticle-enhanced Raman spectroscopy[J]. Langmuir, 2012, 28(24): 9140−9146.

[41] Qiu Z, Zhang M, Wu D Y, Ding S Y, Zuo Q Q, Huang Y F, Shen W, Lin X D, Tian Z Q, Mao B W. Raman spectroscopic investigation on TiO_2-N719 dye interfaces using $Ag@TiO_2$ nanoparticles and potential correlation strategies[J]. ChemPhysChem, 2013, 14(10): 2217−2224.

[42] Li J F, Rudnev A, Fu Y, Bodappa N, Wandlowski T. *In situ* SHINERS at electrochemical single-crystal electrode/electrolyte interfaces: tuning preparation strategies and selected applications[J]. ACS Nano, 2013, 7(10): 8940−8952.

[43] Patnaik P. Handbook of inorganic chemicals[M]. New York: McGraw-Hill, 2003.

[44] Johnson P B, Christy R W. Optical constants of the noble metals[J]. Phys. Rev. B, 1972, 6(12): 4370−4379.

[45] Zwilling M, Schmidt P C, Weiss A. Experimental and theoretical studies of optical properties on alloys of the intermetallic systems $Li_2Ag_{2−x}In_x$ and $Li_2Cd_{2−x}In_x$[J]. Appl. Phys., 1978, 16(3): 255−269.

[46] Huang Y F, Zhang M, Zhao L B, Feng J M, Wu D Y, Ren B, Tian Z Q. Activation of oxygen on gold and silver nanoparticles assisted by surface plasmon resonances[J]. Angew. Chem. Int. Ed., 2014, 53(9): 2353−2357.

[47] Qian J, Xu W, Bhattacharya P, Engelhard M, Henderson W A, Zhang Y, Zhang J G. Dendrite-free Li deposition using trace-amounts of water as an electrolyte additive[J]. Nano Energy, 2015, 15: 135−144.

[48] Xu K. Nonaqueous liquid electrolytes for lithium-based rechargeable batteries[J]. Chem. Rev., 2004, 104(10): 4303−4417.

[49] Aurbach D. Nonaqueous electrochemistry[M]. Marcel Dekker, 1999.

[50] Yang G, Ivanov I N, Ruther R E, Sacci R L, Subjakova V, Hallinan D T, Nanda J. Electrolyte solvation structure at solid-liquid interface probed by nanogap surface-enhanced Raman spectroscopy[J]. ACS Nano, 2018, 12(10): 10159−10170.

[51] Aurbach D, Markovsky B, Shechter A, Ein-Eli Y, Cohen H. A Comparative Study of synthetic graphite and Li electrodes in electrolyte solutions based on ethylene carbonate-dimethyl carbonate mixtures[J]. J. Electrochem. Soc., 1996, 143(12): 3809.

[52] Wang L, Menakath A, Han F, Wang Y, Zavalij P Y, Gaskell K J, Borodin O, Iuga D, Brown S P, Wang C, Xu K, Eichhorn B W. Identifying the components of the solid-electrolyte interphase in Li-ion batteries[J]. Nat. Chem., 2019, 11(9): 789−796.

碳酸酯类电解液中纳米银电极界面过程的原位拉曼光谱研究

谷　宇 [a,#,*]，胡元飞 [a,#]，王卫伟 [a]，尤恩铭 [a]，唐　帅 [a,b]，苏建加 [a]，易　骏 [a]，颜佳伟 [a]，田中群 [a]，毛秉伟 [a,*]

[a] 固体表面物理化学国家重点实验室, 福建能源材料科学与技术创新实验室, 厦门大学化学化工学院, 福建　厦门　361005, 中国
[b] 化学学院, 郑州大学, 河南　郑州　450001, 中国

摘要：

　　锂电池体系中负极表面固态电解质界面相（SEI）对锂电池性能起到至关重要的作用。然而，SEI结构和化学组成复杂，其形成机理至今仍未完全阐明，阻碍了锂电池的发展和应用。本文从方法学角度出发，采用表面增强拉曼光谱（SERS）"借力"策略，通过优化银纳米粒子的结构并借助其外来表面局域等离激元共振作用，开展以EC-DMC为溶剂的碳酸酯类电解液体系中SEI成膜过程的原位研究。为了确保可靠的原位SERS测试，我们设计了一种三电极体系气密拉曼电池。我们利用原位SERS方法，在纳米银电极上获得了SEI成膜过程的组成和结构信息。研究表明，SEI随电位变化呈现出双层结构，其中内层由薄且致密的无机组分构成，外层由疏松的有机组分构成。同时，研究发现LEMC是EC还原的主要成分，而不是LEDC，且金属锂参与的化学反应在形成稳定SEI中的起到关键作用。此外，锂发生沉积后，由于锂与银的合金效应导致其介电常数发生变化，从而削无法进一步增强SEI的拉曼信号。本文为深入理解负极表面SEI的形成及演变过程提供依据，并为今后开展锂电池体系相关界面过程的原位研究提供借鉴。

关键词：固态电解质界面相；原位SERS；负极界面；锂电池